2.25 K_L Simulation Studies with the GlueX Detector

Simon Taylor
Thomas Jefferson National Accelerator Facility
Newport News, VA 23606, U.S.A.

Abstract

Results of simulations of three reactions of interest for a potential K_L program in Hall D at Jefferson Lab, namely $K_L p \to pK_S$, $\pi^+\Lambda$, and $K^+\Xi^0$, are presented.

1. Introduction

The GlueX detector is a large acceptance detector based on a solenoid design with good coverage for both neutral and charged particles. This article describes some simulations of events generated by K_L beam particles interacting with a liquid hydrogen target at the center of the solenoid. The GlueX detector is used to detect one or all of the final state particles. I will be focusing on a few of the simplest two-body reactions, namely $K_L p \to pK_S$, $K_L p \to \Lambda\pi^+$, and $K_L p \to K^+\Xi^0$.

2. Event Generation, Simulation and Reconstruction

The K_L beam is generated by sampling the momentum distribution of K_L particles coming from the decays of ϕ mesons produced by interactions of a photon beam with a beryllium target 16 meters upstream of the liquid hydrogen target. The K_L beam profile was assumed to be uniform within a 2 cm radius at the hydrogen target.

The cross section model for the pK_S channel was determined by parameterizing fits to the existing data for $W \leq 2.17$ GeV and connecting the cross section at $W = 2.17$ GeV to a power-law approximation to the cross section for higher W. The parametrization for low W took the form

$$\frac{d\sigma}{d\Omega} = f_0(W)P_0(\cos\theta) + f_1(W)P_1(\cos\theta) + f_2(W)P_2(\cos\theta), \tag{1}$$

where P_0, P_1, and P_2 are the first three Legendre polynomials and f_0, f_1, and f_2 were determined empirically. The high-W behavior was modeled according to the results reported in Brandenburg *et al.*, [1]: the total cross section falls off as function of the K_L momentum p_K according to $\sigma \propto p_K^{-2.1}$ and the angular dependence for high W depended on $u' = u - u_{max}$, s and t according to

$$\frac{d\sigma}{dt} \propto p_K^{-1.33} e^{(3.1+2.8\log s)t}, \tag{2}$$

$$\frac{d\sigma}{du'} \propto p_K^{-5.24} e^{5.4u'}. \tag{3}$$

The cross section model for the $\Lambda\pi^+$ channel was based on distributions from Yamartino [2].

The cross section model for the $K^+\Xi^0$ channel was based on parametrizations of functions from Jackson *et al.* [3].

The generated events were passed through a full GEANT3-based Monte Carlo of the GlueX detector. The detector consists of a solenoid magnet enclosing devices for tracking charged particles and detecting neutral particles and a forward region consisting of two layers of scintillators (TOF) and a lead-glass electromagnetic calorimeter (FCAL). A schematic view of the detector is shown in Fig. 1. The magnetic field at the center of the bore of the magnet for standard running conditions is about 2 T. The trajectories of charged particles produced by interactions of the beam with the 30-cm liquid hydrogen target at the center of the bore of the magnet are measured using the Central Drift Chamber for angles greater than $\sim 20^{\circ}$ with respect to the beam line. Forward-going tracks are reconstructed using the Forward Drift Chambers. The timing of the interaction of the Kaon beam with the hydrogen target is determined using signals from the Start Counter, an array of 30 thin (3 mm thick) scintillators enclosing the target region. Photons are registered in the central region by the Barrel Calorimeter (BCAL).

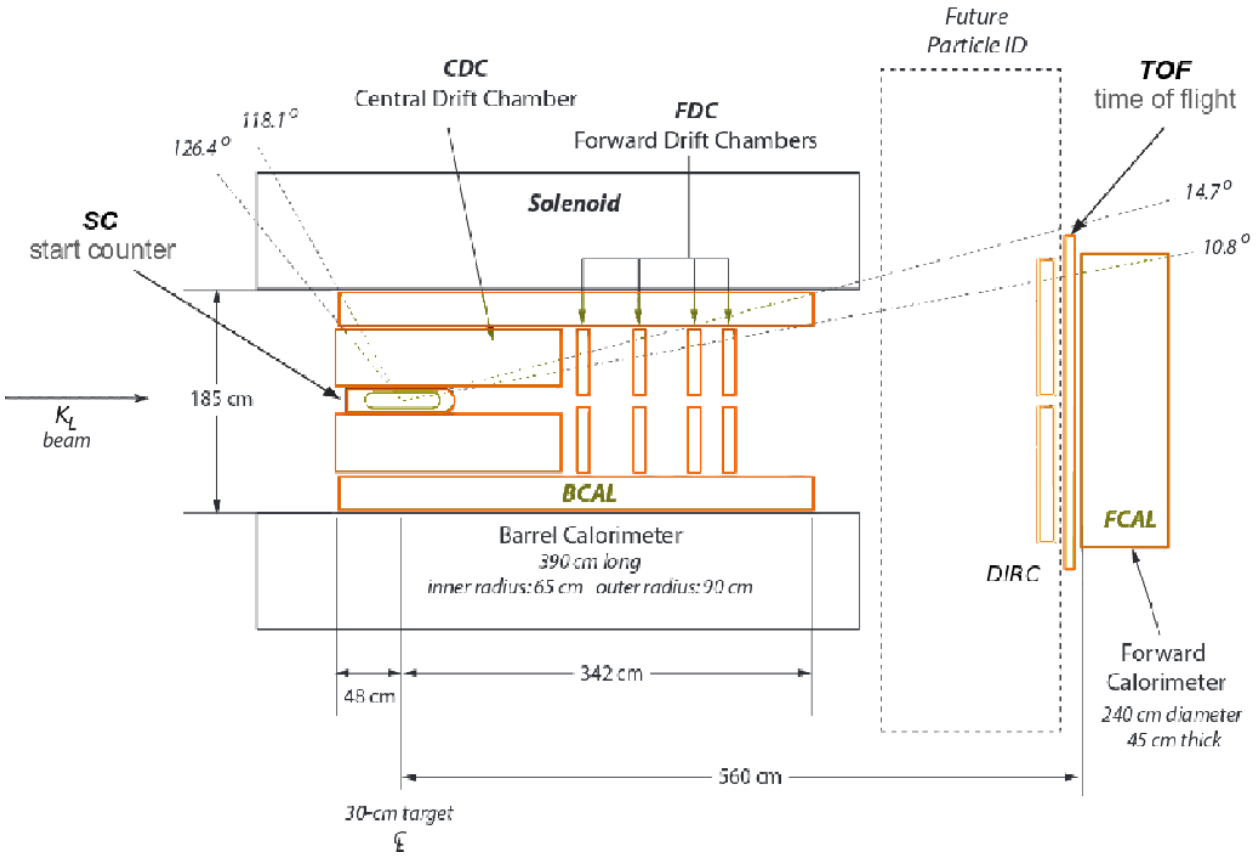

Figure 1: Schematic view of the GlueX detector.

For each topology, one particle (the proton for the pK_S channel, the π^+ for the $\Lambda\pi^+$ channel and the K^+ for the $K^+\Xi^0$ channel) provides a rough determination for the position of the primary vertex along the beam line that is used in conjunction with the start counter to determine the flight time of the K_L from the beryllium target to the hydrogen target. Protons, pions, and Kaons are distinguished using a combination of dE/dx in the chambers and time-of-flight to the outer detectors (BCAL and TOF). The energy loss and timing distributions

for the pK_S channel are shown in Fig. 2; the distributions are similar for the $\Lambda\pi^+$ channel, where a proton band arises from the $\Lambda \to p\pi^-$ decay channel. Also shown is the dE/dx distribution for the $K^+\Xi^0$ channel, where a prominent Kaon band can be seen, along with pion and proton bands arising from Λ decays.

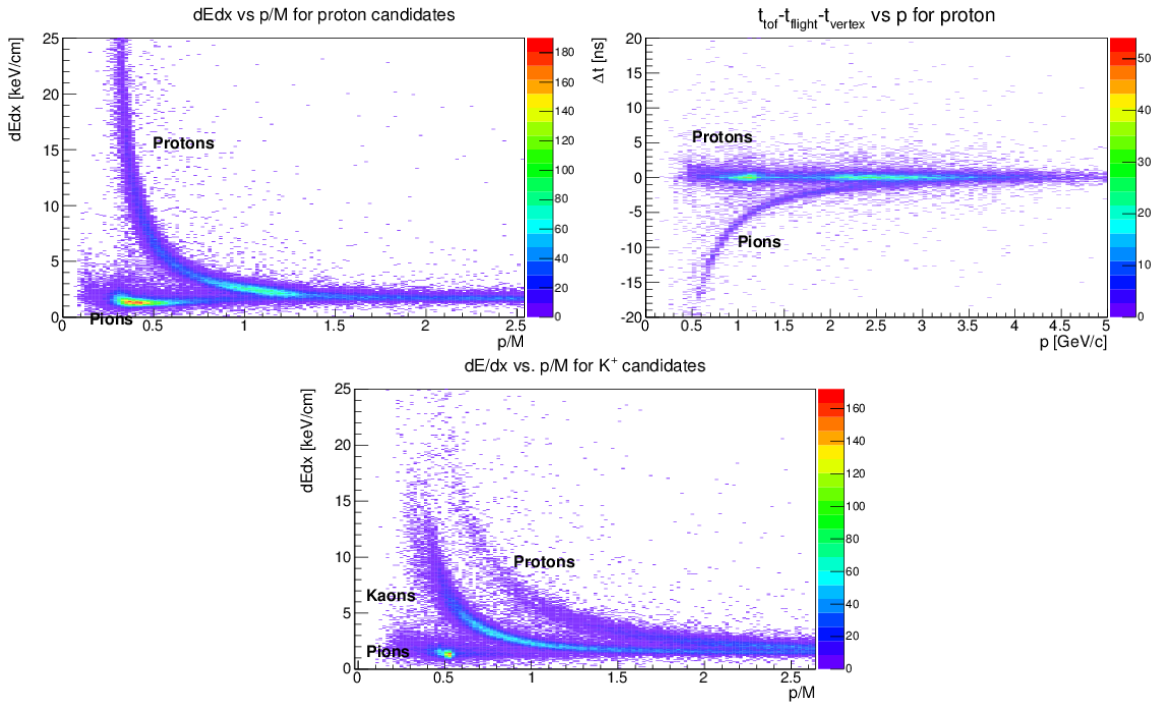

Figure 2: Particle identification: (top left) dE/dx for the pK_S channel; (top right) time difference at the primary "vertex" for the proton hypothesis for the pK_S channel using the TOF; (bottom) dE/dx for the $K^+\Xi^0$ channel. The proton and pion bands arise from the decay of the Λ.

3. Results for each Topology

(a) $K_Lp \to pK_S$

The K_L momentum distribution for the pK_S channel and the mass distribution for the K_S recoiling against the proton are shown in Fig. 3. The missing mass distribution suffers from long non-Gaussian tails.

Since the GlueX detector has full acceptance in ϕ for charged particles and large acceptance in θ (roughly $1^\circ \sim 140^\circ$), reconstruction of full events is feasible. For the pK_S channel, I take advantage of the branching ratio of 69.2% for $K_S \to \pi^+\pi^-$ [4]: the invariant mass of the $\pi^+\pi^-$ pair and W as computed from the four-momenta of the proton and the two pions is shown in Fig. 4. After combining the four-momenta of the final state particles with the four-momenta of the beam and the target, the missing mass squared for the full reaction should be zero, which is also shown in Fig. 4. A comparison between two methods for computing W, one using the K_L momentum and

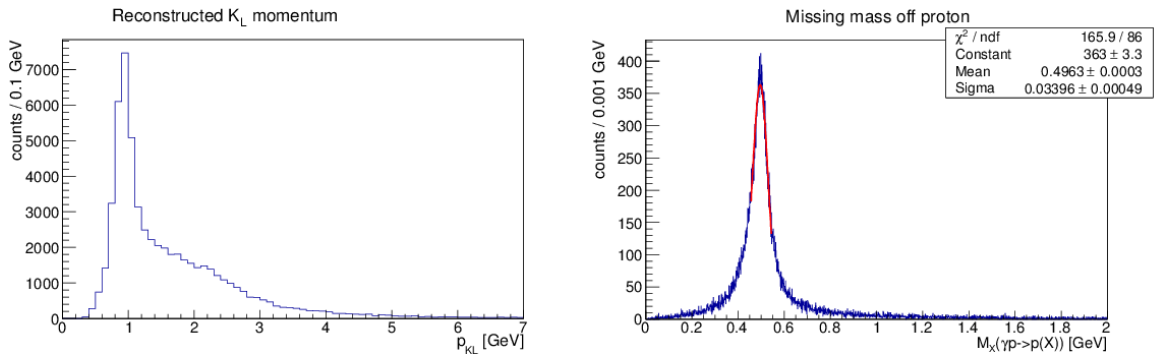

Figure 3: K_L momentum distribution (left) and missing mass off the proton (right) for the pK_S channel.

the other using the final state particles, is shown in Fig. 5. Finally, I require conservation of energy and momentum in the reaction by applying a kinematic fit to the data. After applying a 0.1 cut on the confidence level of the fit, I computed an estimate for the reconstruction efficiency as a function of W as shown in Fig. 6. The efficiency is $\varepsilon = N(W, reconstructed)/N(W, thrown)$. Here the efficiency includes the branching ratio for $K_S \to \pi^+\pi^-$. The average reconstruction efficiency is about 7%.

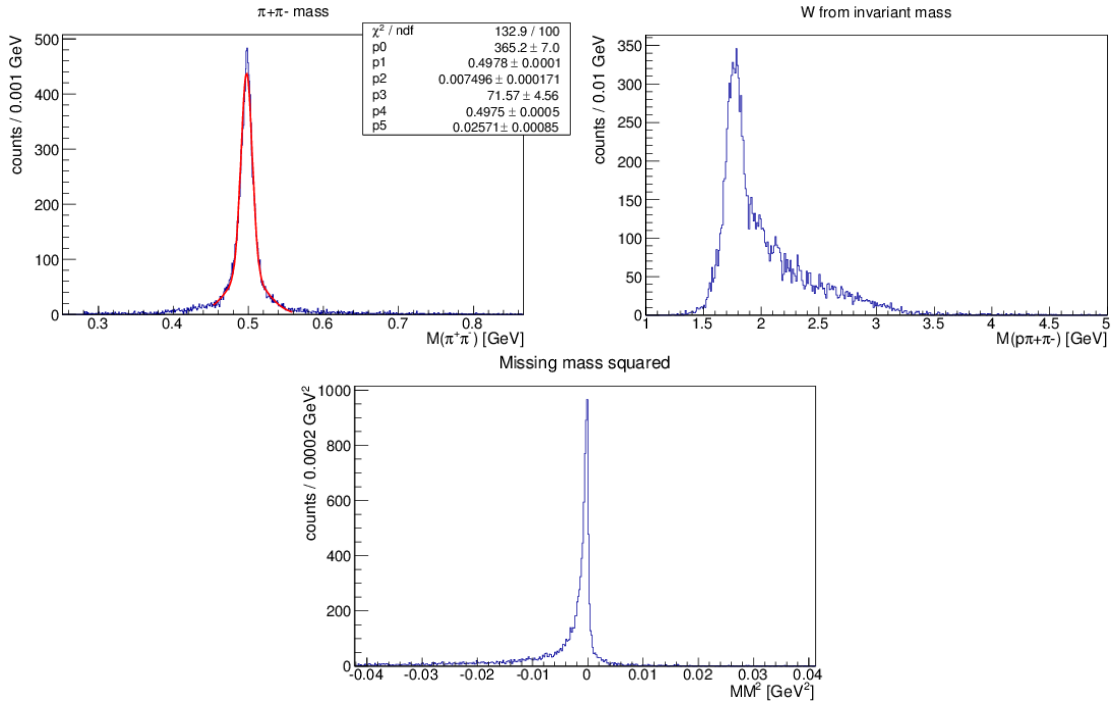

Figure 4: Full reconstruction for $K_L p \to pK_S$, $K_S \to \pi^+\pi^-$: (top left) $\pi^+\pi^-$ invariant mass; (top right) W computed from $p\pi^+\pi^-$ invariant mass; (bottom) missing mass squared for the full reaction.

(b) $K_L p \to \Lambda\pi^+$

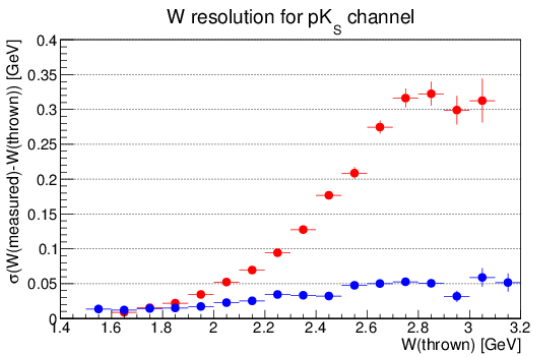

Figure 5: W resolution for the pK_S channel.

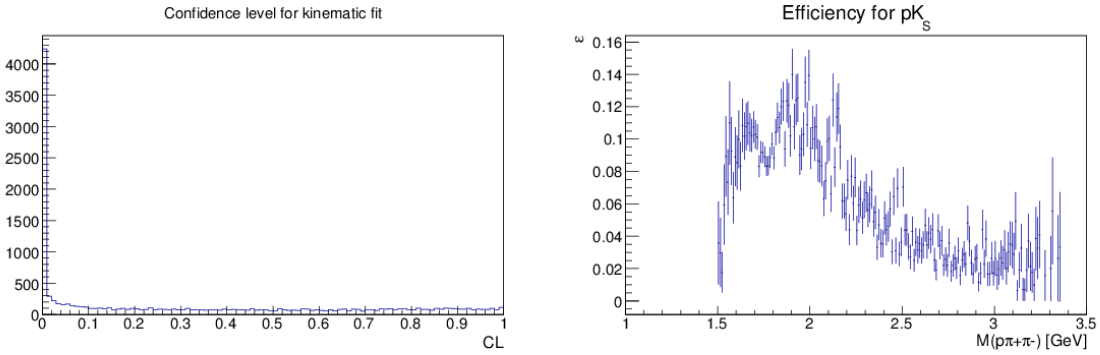

Figure 6: (left) Confidence level distribution for kinematic fit for the pK_S channel. (right) Estimate for efficiency for full reconstruction of the $K_L p \to pK_S$, $K_S \to \pi^+\pi^-$ reaction chain as a function of W.

The reconstructed K_L momentum distribution and the missing mass off the π^+ for the $\gamma p \to \Lambda\pi^+$ simulation are shown in Fig. 7. As with the previous topology, the missing mass distribution has very long non-Gaussian tails.

Taking advantage of the large (63.9%) branching ratio for $\Lambda \to p\pi^-$ [4], the full final state can be reconstructed. The mass distributions for this reaction chain are shown in Fig. 8. A comparison of the W resolution using two methods (one using the K_L momentum and the other using the four-momenta of the final state particles) is shown in Fig. 9. After applying a kinematic fit to the data and cutting at a confidence level of 0.1, I determined the efficiency as a function of W, as shown in Fig. 10. Here the efficiency includes the branching ratio for $\Lambda \to p\pi^-$. The average efficiency is about 2%.

(c) $K_L p \to K^+\Xi^0$

The reconstructed K_L momentum distribution and the missing mass off the K^+ for the $\gamma p \to K^+\Xi^0$ simulation are shown in Fig. 11. The Ξ^0 mass distribution reconstructed using the missing mass technique is broad (full-width-at-half-maximum =$\sim$300 MeV). The Ξ^0 decays almost 100% of the time to $\Lambda\pi^0$ [4]. Here we take advantage of the large branches for $\Lambda \to p\pi^-$ and $\pi^0 \to \gamma\gamma$ to reconstruct Ξ^0's using the four-momenta for all of the final state particles. The reconstructed mass distributions are shown in Fig. 12. A

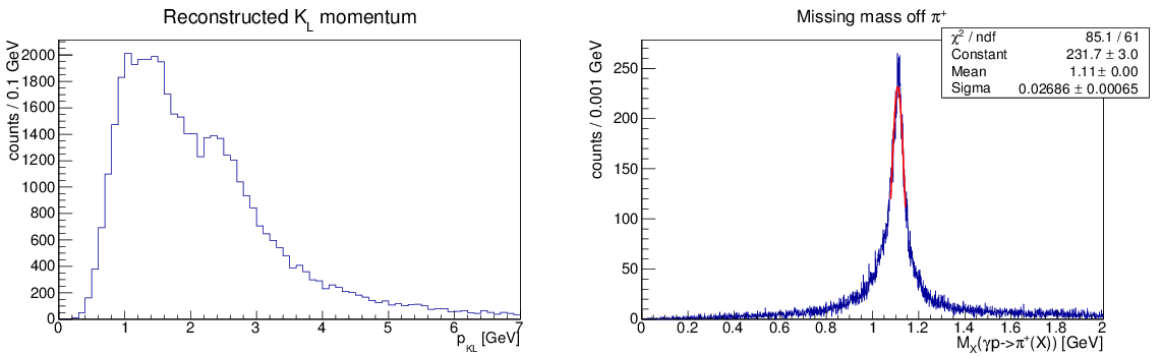

Figure 7: K_L momentum distribution (left) and missing mass off the proton (right) for the $\Lambda\pi^+$ channel.

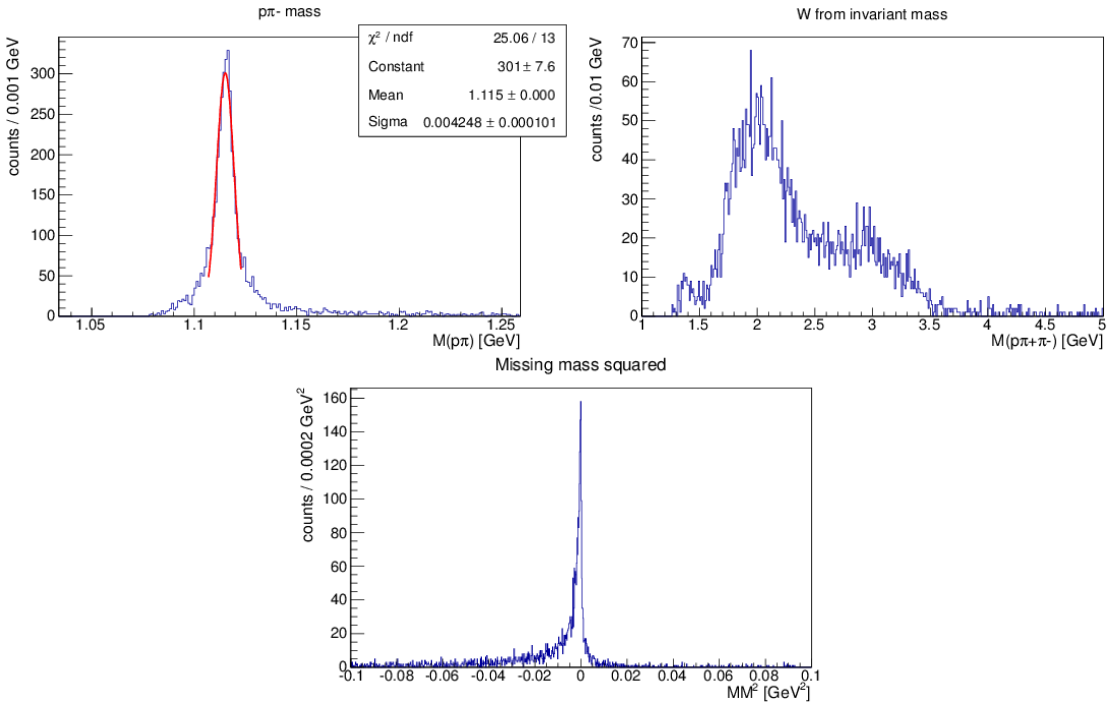

Figure 8: Full reconstruction for $K_L p \rightarrow \Lambda\pi^+$, $\Lambda \rightarrow p\pi^-$: (top left) $p\pi^-$ invariant mass; (top right) W computed from $p\pi^+\pi^-$ invariant mass; (bottom) missing mass squared for the full reaction.

comparison of the two methods for computing W is shown in Fig. 13. An estimate for the efficiency as a function of W after applying a kinematic fit to the data and cutting at a confidence level of 0.1 is shown in Fig. 14. The average efficiency is about 0.4%. This efficiency includes the branching ratios for the Λ and π^0 decays. Also shown is the invariant mass of the Ξ^0 constructed in $p\pi^-2\gamma$. The peak is much narrower than the Ξ^0 peak seen in missing mass.

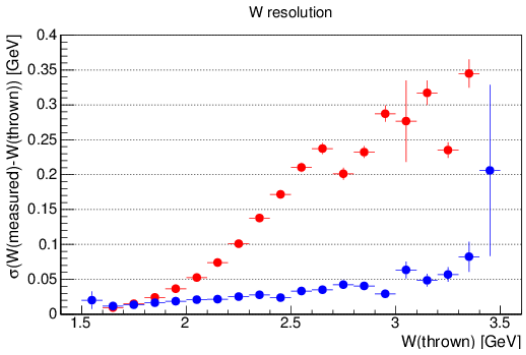

Figure 9: W resolution for the $\Lambda\pi^+$ channel.

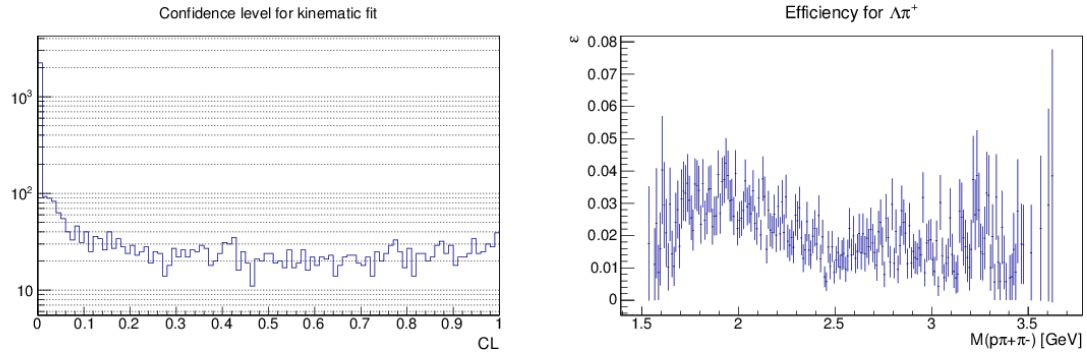

Figure 10: (left) Confidence level distribution for kinematic fit for the $\Lambda\pi^+$ channel. (right) Estimate for efficiency for full reconstruction of the $K_L p \to \Lambda\pi^+, \Lambda \to p\pi^-$ reaction chain as a function of W.

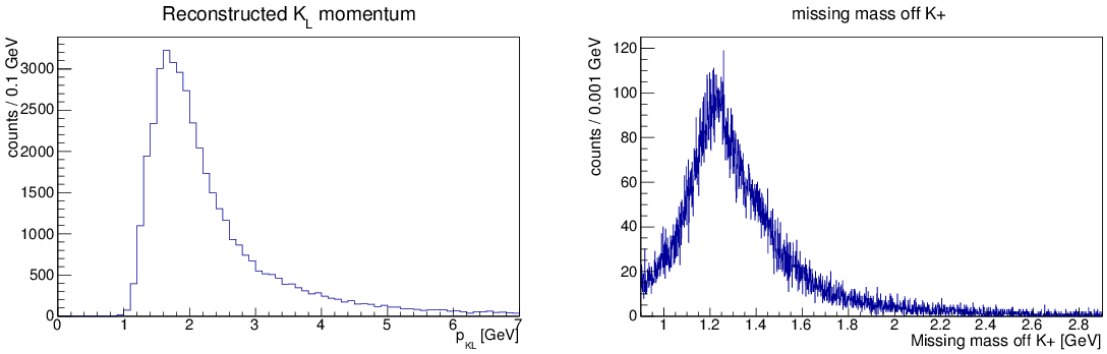

Figure 11: K_L momentum distribution (left) and missing mass off the proton (right) for the $K^+\Xi^0$ channel.

4. **Remarks**

For all topologies under consideration here, the W resolution using the measured K_L momentum worsens considerably as W increases, whereas the W resolution using the final state particles is flatter as a function of W. Resolution at the level of 50 MeV or less can be achieved with the latter technique, at the expense of efficiency. One source for the ineffi-

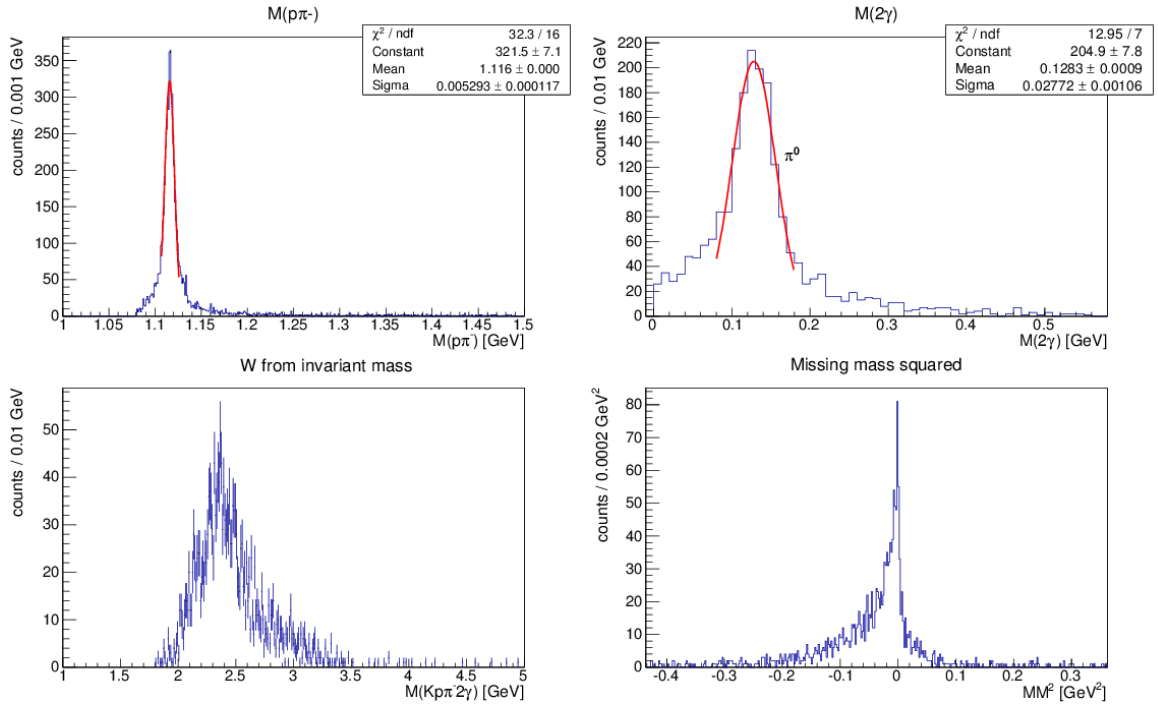

Figure 12: Full reconstruction for $K_L p \rightarrow K^+\Xi^0$, $\Xi^0 \rightarrow \Lambda\pi^0$, $\Lambda \rightarrow p\pi^-$, $\pi^0 \rightarrow \gamma\gamma$: (top left) $p\pi^-$ invariant mass; (top right) two photon invariant mass; (bottom left) W computed from $K^+p\pi^-2\gamma$ invariant mass; (bottom right) missing mass squared for the full reaction.

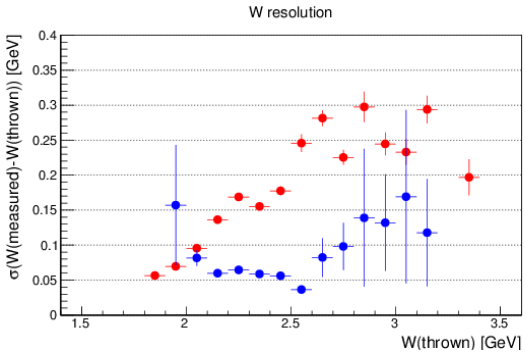

Figure 13: W resolution for the $K^+\Xi^0$ channel.

ciency is the spiraling of low-momentum pions in the magnetic field of the GlueX solenoid, which makes track finding and fitting difficult. This can be mitigated by running the solenoid at a lower current than the standard current for regular GlueX runs. The preliminary kinematic fitting results are encouraging and further improvement in the W resolution can be expected for the case where events are fully reconstructed.

5. Acknowledgments

The author would like to thank Ilya Larin for providing event generation code and Mark

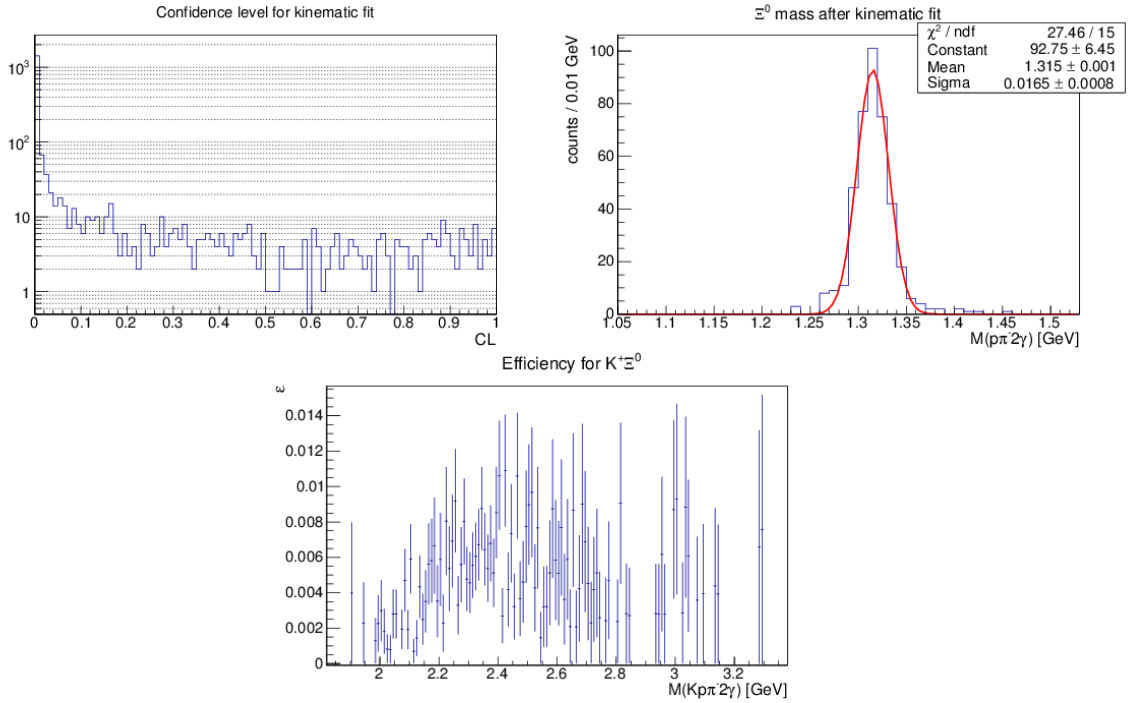

Figure 14: (top left) Confidence level distribution for kinematic fit for the $K^+\Xi^0$ channel. (top right) Ξ^0 mass distribution after kinematic fit with a 0.1 confidence level cut. (bottom) Estimate for efficiency for full reconstruction of the $K_Lp \rightarrow K^+\Xi^0$, $\Xi^0 \rightarrow \Lambda\pi^0$, $\Lambda \rightarrow p\pi^-$, $\pi^0 \rightarrow \gamma\gamma$ reaction chain as a function of W.

Manley for providing plots of cross section data for the $K_Lp \rightarrow pK_S$ reaction. This material is based upon work supported by the U.S. Department of Energy, Office of Science, Office of Nuclear Physics under contract DE–AC05–06OR23177.

References

[1] G.W. Brandenburg *et al.*, Phys. Rev. D **9**, 1939 (1974).

[2] R. Yamartino, Ph.D. Thesis, SLAC (1974); SLAC-R-0177.

[3] B.C. Jackson, Y. Oh, H. Haberzettl, and K. Nakayama, Phys. Rev. C **91**, 065208 (2015).

[4] K.A. Olive *et al.* (Particle Data Group), Chin. Phys. C **38**, 090001 (2014).